Materials Horizons

Accepted Manuscript

This article can be cited before page numbers have been issued, to do this please use: X. Song, H. Wang, C. Gan, R. Yuan and Y. Xiang, *Mater. Horiz.*, 2025, DOI: 10.1039/D5MH00811E.

ROYAL SOCIETY OF CHEMISTRY

rsc.li/materials-horizons

View Article Online
DOI: 10.1039/D5MH00811E

COMMUNICATION

In situ partial vulcanization synthesis of conductive and highly catalytic bimetal organic framework for sensitive electrochemical cancer-specific neoantigen detection

Received 00th January 20xx,
Accepted 00th January 20xx

DOI: 10.1039/x0xx00000x

Xinmei Song [a], Hao Wang [a], Chunfang Gan *[b], Ruo Yuan [a] and Yun Xiang *[a]

Neoantigens are unique tumor-derived epitopes to facilitate the development of immunotherapeutic interventions and advance the precision diagnosis of cancers. However, it remains significant challenges to detect these neoantigens due to their inert electrochemical/fluorescent properties and low abundance, and mass spectroscopy is currently the prevailing neoantigen analysis platform constrained by procedural complexity, prohibitive cost, and isotopic tagging. On the basis of in situ partial vulcanization synthesis of a new conductive bimetal organic framework and the peptide derivatization strategy, we demonstrate an innovative catalysis-enhanced electrochemical neoantigen biosensing platform for direct and specific electrochemical cancer diagnosis. The bimetallic sulfide nanoparticle-decorated conductive MOF nanocomposite (NiCo-MS/c-MOF) is synthesized and shows considerably enhanced electrocatalytic activity. Upon the conversion of the neoantigen to electroactive molecules via isoindole derivatization, significantly amplified catalytic current can be obtained on NiCo-MS/c-MOF-modified electrode to realize sensitive detection of the KRAS G12D neoantigen down to 0.6 nM. In addition, the monitoring of trace KRAS G12D neoantigen in complex with human leukocyte antigens (HLAs) on cancer cells has also been verified, highlighting the promising potential of our methodology for precise and early diagnosis of cancers.

New concepts

We show the in situ partial vulcanization synthesis of a new bimetallic sulfide nanoparticle-decorated conductive MOF nanomaterial (NiCo-MS/c-MOF) with ultrahigh electro-catalytic activity toward the oxidation of isoindole derivatizatied peptides. Such NiCo-MS/c-MOF shows excellent conductivity and catalytic activity against conventional MOF materials. Furthermore, the application of this new material for the construction of the first example of the electrochemical sensing interface for neoantigen peptide, a newly discovered and exclusive cancer-specific type of molecular biomarker for precise cancer diagnosis, has also been demonstrated as well. Due to the high performance of the NiCo-MS/c-MOF material, we are able to detect specific KRAS G12D neoantigen in cancer cell lysate with high sensitivity, thereby suggesting the promising insights for the synthesis of new and high performance bimetallic nanocomposite materials for robust biomedical and biological applications.

1. Introduction

Biomarker-based cancer diagnosis is typically achieved by measuring abnormal changes in biomolecular levels in human body fluids.[1,2] However, in the early stages of the diseases, biomarkers are present in trace amounts and are prone to raising a high risk of false-positive signals due to the background generated by normal cells.[3] To minimize or even eliminate false positives, detection of biomarkers that are produced and secreted only by cancer cells is important to achieve precise cancer diagnosis. Neoantigens, a class of short peptides composed of 8 ~ 20 amino acids, are derived from tumor-specific genetic mutations and delivered to cancer cell surfaces by human leukocyte antigen (HLA). These neoantigens exist as HLA-restricted neoantigens complexes on the cell surfaces and can induce specific T cell-mediated immune responses.[4,5] Unlike common cancer-related antigens (TAAs) that are abnormally produced by cancer cells but also exist at low levels in normal

[a] Key Laboratory of Luminescence Analysis and Molecular Sensing, Ministry of Education, School of Chemistry and Chemical Engineering, Southwest University, Chongqing 400715, PR China.
[b] Guangxi Key Laboratory of Natural Polymer Chemistry and Physics, College of Chemistry and Materials Science, Nanning Normal University, Nanning 530001, PR China
Email: yunatwu@swu.edu.cn (Y. Xiang); ganchunfang2008@126.com (C. Gan)
† Supplementary Information available. See DOI: 10.1039/x0xx00000x

cells, neoantigens generated by hotspot mutations in cancer genes are specific to tumor cells.[6] The unique cancer cell specificity of neoantigens makes them promising target candidates for precise immunotherapy to avoid the risk of off-target toxicity caused by TAAs-directed therapy, and holds substantial potential as biomarkers for cancer diagnosis and predicting patient response to cancer immunotherapy.[7,8] Therefore, establishment of analytical approaches for the identification and determination of neoantigens can significantly promote accurate diagnosis of diseases and precise immunotherapy.

Nevertheless, the short peptide sequences and low abundance of neoantigens pose significant challenges in establishment of assays for analyzing HLAs-restricted neoantigens. Although monitoring the proliferation of neoantigen-reactive T cells can indirectly estimate the amount of neoantigens presented on the cell surface, the whole process is time-consuming and labor-intensive.[9] Mass spectrometry is currently the most common technology for analysis of neoantigens presented on the cell surface, which typically includes enriching neoantigens from cell lysates through immunoprecipitation purification (IP), followed by chromatographic separation and mass spectrometry analysis to identify their respective abundance.[10] Furthermore, the preparation of isotopically tagged reference analytes for Mass spectrometry-based quantification necessitates concurrent development of large-scale peptide libraries encompassing hundreds of variants to optimize analytical parameters, collectively introducing substantial technical complexity and assay costs throughout the workflow.[11,12] Therefore, the establishment of efficient methods that simplify the identification process while ensuring the accurate detection of HLA-restricted neoantigens remains a major challenge.

Previous studies have demonstrated that small peptides containing primary amines can react with o-phthaldialdehyde/2-mercaptoethanol (OPA/2-ME) ligand to form electroactive or fluorescent isoindole derivatives,[13,14] providing a simple and more effective approach to analyze linear short peptides using electrochemical techniques or fluorescence means. The electrochemistry-based approach has garnered lots of attentions due to its inherent superiority of rapid response, simplicity, low cost, and high sensitivity for the analysis of trace substances.[15] Furthermore, peptides-derived isoindole compounds may exhibit self-quenching effects that disturb fluorescence measurements, whereas causing no effect on electrochemical response,[16] making electrochemical assays particularly well-suited for peptide analysis.

Detection of low abundance of peptides imposes high sensitivity requirement on electrochemical sensors. Modification of active catalysts, including metal nanoparticles, carbon-based materials, metal oxide nanoparticles, polymers, and composite materials, on the electrode interfaces to enhance electron transfer kinetics and active site accessibility is a well-established approach to improve the analytical sensitivity.[17,18] These catalysts have enabled the sensitive electrochemical analysis of various biological molecules, e.g., dopamine, ascorbic acid, and serotonin.[19-21] Among these materials, metal-organic frameworks (MOFs), a subclass of coordination polymers assembled from metal clusters and organic linkers,[22] are considered as the promising functional catalysts for electrochemical sensing, due to their superior features of highly ordered structures, large surface areas, and porosities. However, wide electrochemical applications of most MOFs are restricted because of their poor conductivity and slow mass transfer processes.[23] Conductive MOFs (c-MOFs) comprising transition metallic nodes (Co, Ni, Cu) linked by benzene-, triphenylene-, or phthalocyanine-based ligands have been developed to overcome this limitation.[24] The unique π-conjugated 2D planar structure of c-MOFs imparts them with properties similar to graphene, resulting in excellent conductivity over other MOFs, and thereby enabling extensive applications in energy storage, electrocatalysis and sensing applications.[25] The *in situ* introduction of heterogeneous species into MOFs, such as metal phosphides, metal sulfides, and metal oxide nanoparticles, can modulate the nanostructure of MOFs to increase their active surface area and intrinsic conductivity, as well as improve the inherent electrocatalytic activity by exerting synergistic effects among different constituents through interfacial electronic coupling or defect formation.[26-28] Among these heterogeneous species, metal sulfides are particularly notable due to their strong metal-sulfur bridging bonds and numerous sulfur vacancies, which confer excellent electrical conductivity and catalytic activity to accelerate the electrode reactions,[29,30] thereby holding significant promise for improving the analytical performance of electrocatalytic biomolecules determination.

Here, we report an ultrasensitive electrochemical neoantigen sensor with a new, highly conductive and catalytic bimetallic sulfide nanoparticle-decorated MOF nanocomposite (NiCo-MS/c-MOF) coupled with the isoindole derivatization strategy. The KRAS G12D neoantigen, arising from a glycine-to-aspartate substitution at codon 12 within the KRAS proto-oncogene locus, is employed as the model analyte. The KRAS G12D neoantigen is a dominant driver mutation in gastrointestinal malignancies with a mutational prevalence of 60-70% in pancreatic adenocarcinomas and 20-30% in colorectal carcinoma,[31,32] has been validated as a molecularly defined diagnostic biomarker for cancer diagnosis. With the assistance of OPA/2-ME ligand, the KRAS G12D neoantigens are converted to electroactive isoindole derivatives, which can be oxidized on NiCo-MS/c-MOF-modified electrode to yield substantially amplified catalytic current. This leads to the detection of trace KRAS G12D neoantigens and enables unambiguous identification and quantification of HLA-restricted KRAS G12D in cell lysates.

2. Results and discussion

2.1 Principle description of amplified electrochemical neoantigen assay.

A dual-stage solvothermal protocol for preparing the NiCo-MS/c-MOF and an electrocatalytic biosensing methodology for ultrasensitive KRAS G12D neoantigen quantification are outlined in Scheme 1. The rod-shaped 2D conductive NiCo-MOF (c-MOF) is formed through a coordination-driven self-assembly reaction

between metallic nodes (Ni and Co) and highly π-conjugated hexatopic triphenylene-based ligand (HHTP) (Scheme 1A). Subsequently, the c-MOF is partially vulcanized by Na_2S to generate metal sulfide nanoparticles on the surface of MOF to obtain NiCo-MS/c-MOF, which is then drop-cast onto GCE to prepare the conductive and highly electrocatalytic sensing interface for KRAS G12D detection. Because the KRAS G12D (VVGADGVGK) is non-electroactive, a derivative step is therefore employed to transform it into an electroactive isoindole product by using OPA/2-ME ligand (Scheme 1B). In the typical derivative process (Scheme 1C), OPA undergoes cyclocondensation with the α-amino moiety of the KRAS G12D neoantigen, generating a metastable isoindole-based Schiff base intermediate. This intermediate exhibits enhanced nucleophilic reactivity to enable rapid reaction with the thiol group of 2-ME, yielding electroactive 1-thiol isoindole derivative with high efficiency. The KRAS G12D neoantigen can thus subsequently be quantified with high sensitivity on NiCo-MS/c-MOF/GCE via catalytic electrooxidation of the isoindole derivatives for yielding significantly amplified currents.

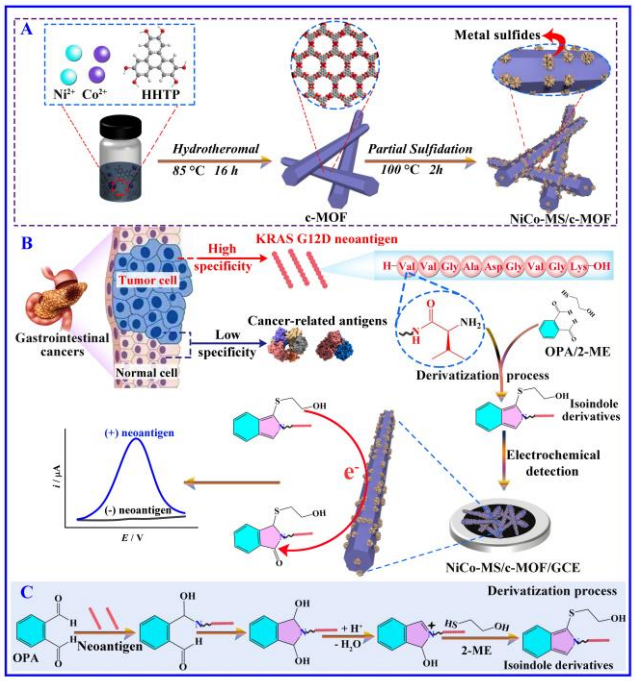

Scheme 1. Description of (A) the synthetic pathway for NiCo-MS/c-MOF, (B) electrocatalytic detection of KRAS G12D neoantigen, and (C) OPA/2-ME-mediated derivatization process of neoantigen.

2.2 Structure and morphology characterizations of NiCo-MS/c-MOF.

The nanostructure and compositional information of NiCo-MS/c-MOF were first elucidated by typical characterization techniques. The scanning electron microscope (SEM) images (Fig. 1A and 1B) indicate that the synthesized c-MOF exhibit distinct rod-shaped structure with length of approximately 400 nm and diameters of 40~70 nm. After c-MOF is vulcanized by Na_2S for 2 h to NiCo-MS/c-MOF, the rod-shaped morphology and dimensions are maintained without obvious changes while the surface becomes notably rougher (Fig. 1C and 1D). Transmission electron microscopy (TEM) characterization (Fig. 1E and 1F) reveals uniform dispersion of ~2 nm nanoparticles across the c-MOF surface. High-resolution (HRTEM) analysis (Fig. 1G) of NiCo-MS/c-MOF exhibits the lattice distance of 1.91 nm, indexed to the (010) crystal plane of c-MOF.[33] Fig. 1H displays two distinct lattice spacing of 0.29 nm and 0.26 nm, which are coincided with (100) crystal plane of NiS and (102) crystal plane of CoS, respectively.[34,35] Furthermore, elemental mapping through energy-dispersive X-ray spectroscopy (EDS) of the NiCo-MS/c-MOF composite, as shown in Fig. 1I, verifies the existence of C, O, Ni, Co, and S elements.

Powder X-ray diffraction (PXRD) technique was also performed to determine chemical composition and crystal structures of synthesized materials (Fig. 2A). The PXRD pattern of c-MOF exhibits diffraction peaks at 4.7°, 9.6°, 13.8°, 16.2°, 26.7°, and 27.0°, which belong to the (010), (020), (121), (022), (004), and (014) planes of c-MOF (NiCo-HHTP), respectively.[36] The XRD diffraction peak positions of c-MOF closely match the simulated pattern of Ni-MOF (Ni-HHTP), confirming its high phase purity and good crystallinity. Besides, these diffraction peaks of c-MOF are retained in the PXRD pattern of NiCo-MS/c-MOF with additional diffraction peaks at 30.1°, 33.2°, and 34.4° ascribed to (100), (002), and (101) crystal planes of NiS (JCPDS No. 89-1956), and the new peaks at 35.3°, 46.9°, and 54.2° match well with the (101), (102), and (110) crystal planes of CoS (JCPDS No. 75-0605). These results therefore confirm the successful incorporation of bimetallic sulfides into the c-MOF structure. The surface chemical states of NiCo-MS/c-MOF were further analyzed using X-ray photoelectron spetroscopy (XPS). The survey spectrum of NiCo-MS/c-MOF proves presence of Ni, Co, C, O, and S elements (Fig. 2B). Four deconvoluted peaks at 284.8 eV, 286.6 eV, 288.1 eV, and 290.7 eV are identified in C 1s spectrum (Fig. S4A), corresponding to C-C, C-O, C=O bonds, and π–π* satellite peak originating from the termination of the coordination-unsaturated catecholates, respectively.[37] For O 1s spectrum (Fig. S4B), fitting peaks at 531.1 eV, 532.7 eV, and 535.5 eV belong to metal (Ni and Co)-O, C–O and H_2O, respectively.[38] The Ni 2p spectrum (Fig. 2C) reveals characteristicpeaks at 855.9 eV and 873.7 eV, which are respectively assignable to the Ni $2p_{3/2}$ and Ni $2p_{1/2}$ of Ni^{2+}.[39] In spectrum of Co 2p (Fig. 2D), binding energies of 781.1 eV and 796.6 eV are assigned to Co $2p_{3/2}$ and Co $2p_{1/2}$, indicating presence of Co^{2+} species in NiCo-MS/c-MOF.[40] Moreover, the characteristic peaks for S 2p at 163.7 eV and 165.0 eV can be attributed to S $2p_{3/2}$ and S $2p_{1/2}$ of S^{2-} (Fig. 2E), and the peaks at 168.0 eV and 169.3 eV correspond to residual sulfate species resulting from surface oxidation during the vulcanization reaction.[41] Nitrogen adsorption–desorption analysis (Fig. S5) reveals that NiCo-MS/c-MOF possesses a mesoporous structure with considerable surface area and hierarchical pores, which are beneficial for enhancing mass transport and improving electrochemical accessibility of active sites.

View Article Online
10.1039/D5MH00811E

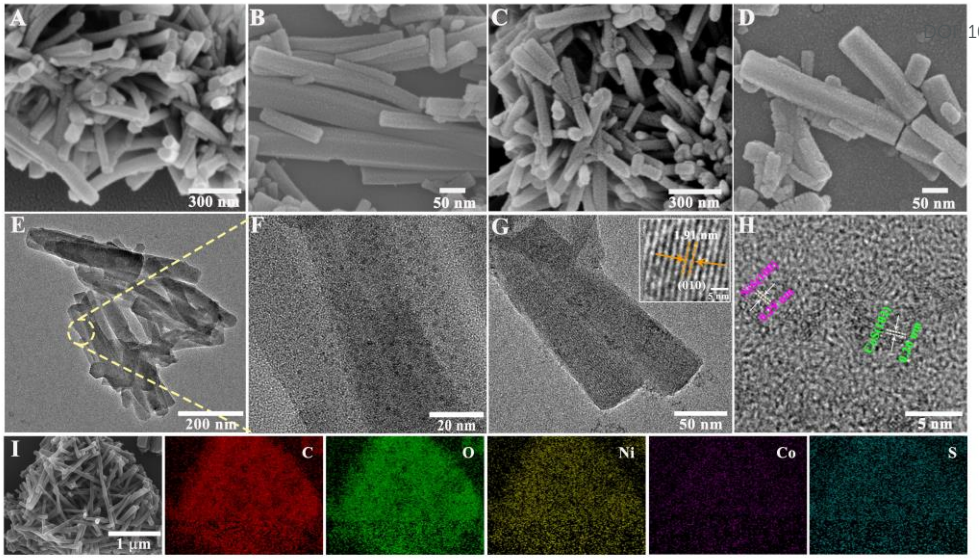

Fig. 1 SEM images c c-MOF.

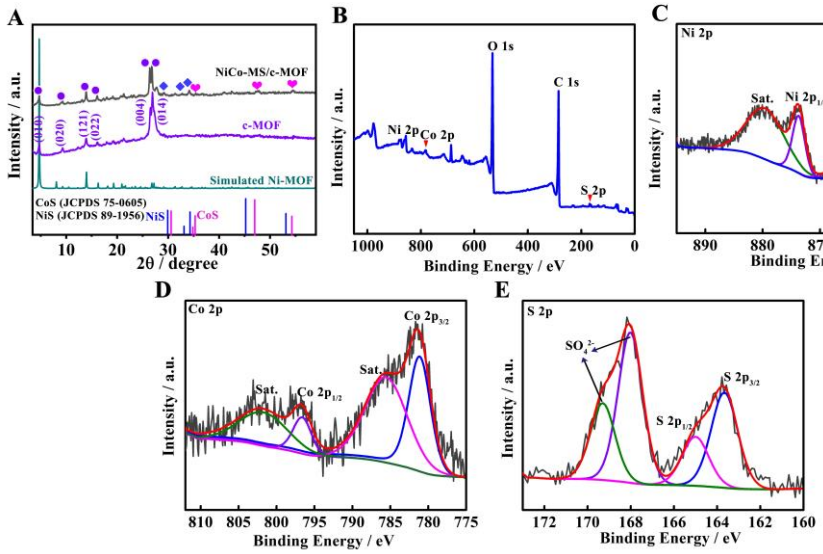

Fig. 2 (A) PXRD patterns of c-MOF (NiCo-HHTP), NiCo-MS/c-MOF, and simulated Ni-MOF (Ni-HHTP); XPS spectra of NiCo-MS/c-MOF, include (B) survey scan, (C) Ni 2p, (D) Co 2p, and (E) S 2p.

2.3 Evaluation of electrochemical behaviors of NiCo-MS/c-MOF/GCE.

The electrochemical behaviors of NiCo-MS/c-MOF/GCE were systematically investigated using $[Fe(CN)_6]^{3-/4-}$ as electroactive probes. As evidenced by the cyclic voltammograms (CV) in Fig. 3A, the bare GCE (curve a) features with two symmetrical and well-defined redox peaks, whereas the introduction of conductive c-MOF induces slight attenuation in peak current intensity accompanied by minor broadening of the peak potential separation (curve b). Such observation can be attributed to the negatively charged c-MOF exhibits reduced reactivity towards $[Fe(CN)_6]^{3-/4-}$.[42] However, the peak currents of NiCo-MS/c-MOF/GCE are obviously enhanced compared with bare GCE and c-MOF/GCE (curve c), suggesting that incorporation of metal sulfides can significantly enhance conductivity of c-MOF. The NiCo-MS/GCE (curve d) exhibits enhanced conductivity compared to bare GCE and c-MOF/GCE, while it is inferior to NiCo-MS/c-MOF/GCE. The EIS results in Fig. 3B also reveal that the charge transfer resistance (R_{ct}) of NiCo-MS/c-MOF/GCE is smaller than that of NiCo-MS/GCE, c-MOF/GCE, and bare GCE, which is in accordance with the CV measurements. In addition, electrochemical active surface area (ECSA) of nanomaterial-modified/bare GCE was also evaluated through comparative analysis of double layer capacitance (C_{dl}) derived from the non-Faradaic potential window of their CV curves recorded in KOH solution. Typical CV curves of different materials with different scan rate are displayed in Fig. S6. Linear slope obtained by plotting the difference of charging current density versus scan rate represents twice of C_{dl}, which is directly proportional to ECSA.[43] As depicted in Fig. 3C, NiCo-MS/c-MOF/GCE exhibits a significantly higher C_{dl} compared to c-MOF/GCE and bare GCE counterparts, indicating that the metal sulfides-embedded c-MOF possesses increased surface area for interacting with electrolyte and abundant active sites for electrocatalytic activity.

View Article Online
DOI: 10.1039/D5MH00811E

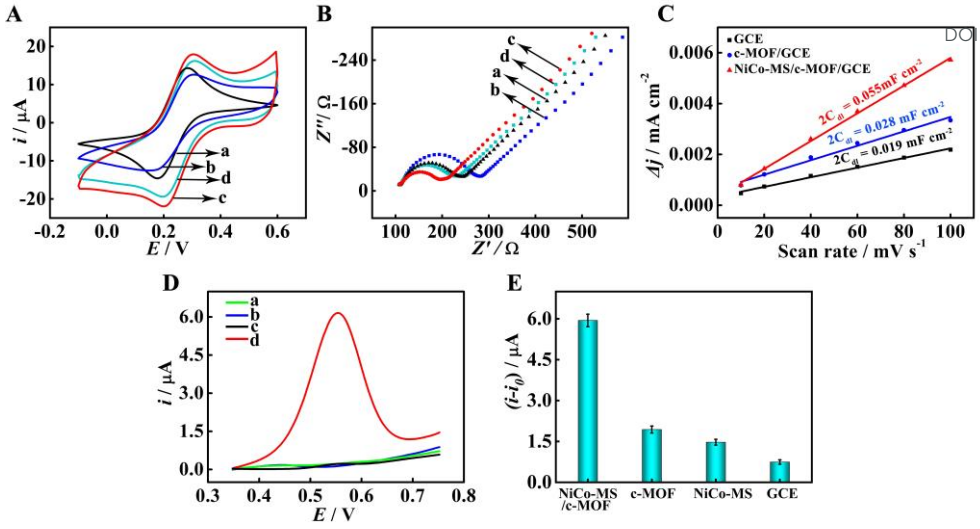

Fig. 3 (A) CV and (B) EIS of (a) bare GCE, (b) c-MOF/GCE, (c) NiCo-MS/c-MOF/GCE, and (d) NiCo-MS/GCE in 0.1 M KCl solution containing $[Fe(CN)_6]^{3-/4-}$; (C) Scan rate-dependent anodic-cathodic current density differential Δj (j_a - j_c) for the three electrodes (10 ~ 100 mV s^{-1}), where j_a and j_c denote peak current densities at the selected potential; (D) SWV curves obtained on NiCo-MS/c-MOF/GCE in different solutions: (a) PBS, (b) KRAS G12D + PBS, (c) OPA/2-ME + PBS, (d) KRAS G12D + OPA/2-ME + PBS; (E) Comparative analysis of the electrocatalytic performance across nanocomposite-functionalized electrodes for KRAS G12D neoantigen quantification. Following a 6-minute derivatization protocol (10 μL of 500 nM KRAS G12D with 20 μL of 100 μM OPA/480 μM 2-ME in methanol, diluted in 970 μL PBS [pH 7.4]), the processed solution was subjected to SWV analysis. Error bars: SD, n = 3.

2.4 Exploration of electrocatalytic activity of NiCo-MS/c-MOF/GCE.

The electrocatalytic behavior of NiCo-MS/c-MOF/GCE toward KRAS G12D neoantigen was investigated by square wave voltammetry (SWV). As shown in Fig. 3D, NiCo-MS/c-MOF/GCE exhibits no noticeable current in PBS solution (curve a), demonstrating the NiCo-MS/c-MOF nanocomposite is stable without causing intrinsic electrochemical interference peaks within the detection potential window. When 500 nM of KRAS G12D neoantigen was added to PBS solution, almost no change in current can be observed (curve b), revealing that KRAS G12D is non-electroactive. Similarly, the NiCo-MS/c-MOF/GCE shows negligible current peaks in PBS solution containing OPA/2-ME ligand (curve c), whereas a significantly enhanced current peak at 0.57 V is obtained after the derivatization of KRAS G12D neoantigen by OPA/2-ME ligand (curve d). The substantial difference in electrochemical behavior confirms the engineered catalytic interface can enable the ultrasensitive determination of KRAS G12D neoantigens. Further validation through controlled experiments with bare GCE, c-MOF/GCE, and NiCo-MS/GCE were also performed (Fig. S7). By calculating SWV peak current difference between presence (i) and absence (i_0) of KRAS G12D in PBS with the OPA/2-ME ligand, it can be seen in Fig. 3E that electro-oxidation current response generated on NiCo-MS/c-MOF/GCE shows about 307% increase than that observed on c-MOF/GCE, 404% higher than NiCo-MS/GCE, and is significantly enhanced compared with bare GCE. The significantly lowered current response of NiCo-MS/GCE vs. NiCo-MS/c-MOF/GCE stems from structural collapse of the original c-MOF during its complete sulfidation to NiCo-MS, as confirmed by SEM and XRD characterization (Fig. S8), resulting in catalytic activity inhibition.[44,45] These results demonstrates that c-MOF can facilitate electrocatalytic sensing of KRAS G12D and *in situ* introduction of metal sulfides can further enhance the catalytic activity of c-MOF.

2.5 Optimization of KRAS G12D neoantigen sensing conditions.

Experimental conditions, including the concentration of OPA/2-ME solution and the reaction time for derivatization, were investigated by SWV measurements to optimize the electrocatalytic analysis of KRAS G12D. The concentration of the OPA/2-ME solution was optimized by examining influence of different OPA concentration upon SWV current response with maintaining concentration ratio of OPA to 2-ME at 1:4.8. The results reflected in Fig. 4A demonstrate that the peak current exhibits an elevated trend with increasing concentration of OPA from 25 μM to 250 μM, and reaches saturation at 200 μM, suggesting that an OPA concentration of 200 μM coupled with 960 μM of 2-ME is sufficient to complete the derivatization reaction. Further investigation into the reaction time for derivatization reveals that the peak current gradually increases with reaction time to 9 min, after which it slightly declines (Fig. 4B). This behavior is attributed to decreased stability of isoindole products generated from the derivatization reaction between OPA/2-ME and primary amines of peptides.[46] Therefore, derivatization time of 9 min was selected as the optimum.

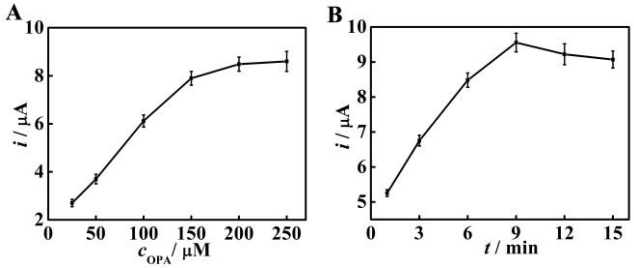

Fig. 4 Effects of (A) the concentration of OPA/2-ME solution and (B) KRAS G12D derivatization time on SWV response. Error bars: SD, n = 3.

2.6 Quantitative electrochemical detection of KRAS G12D neoantigen.

The sensitivity of the established sensor for the analysis of KRAS G12D neoantigen was assessed under optimal conditions. The results in Fig. 5A illustrate that peak current increases progressively as KRAS G12D concentration is elevated. Quantitative analysis of SWV responses in Fig. 5B establishes a biphasic calibration profile spanning two distinct regimes: 1 ~ 50 nM (i = 0.0828 c + 0.7136, R^2 = 0.9961) and 50 nM ~ 1 μM (i = 0.0097 c + 4.5857, R^2 = 0.9968), where current intensity (i) correlates linearly with KRAS G12D neoantigen concentration (c). The observed dual linearity in the quantitative relationship is primarily attributed to the reaction kinetics variations at different neoantigen concentrations. At low concentrations, sufficient electrode active sites enable efficient electron transfer with a linear, sensitive response. At elevated concentrations, site saturation occurs while electro-oxidation generates electrochemically inactive products to adsorb onto the electrode surface, which causes partial surface blockage, impeding electron transfer and resulting in a second linear region with a different slope.[47,48] Additionally, the biosensing platform achieves a detection limit of 0.6 nM for KRAS G12D neoantigen based on 3σ criteria. Compared with previously reported methods, the proposed sensor exhibits a lower detection limit and a wide linear range (Table S1). Reproducibility assessments via six trials at 500 nM concentration of neoantigen exhibits acceptable signal variance (RSD = 5.1%). The stability of the NiCo-MS/c-MOF/GCE was also evaluated by storing the modified electrodes at room temperature up to 4 weeks, followed by performing electrochemical measurements for KRAS G12D neoantigen at 500 nM. Fig. 5C demonstrates that the NiCo-MS/c-MOF/GCE retains 92.7% of its initial SWV response after 28-day storage, indicating that the NiCo-MS/c-MOF/GCE exhibits acceptable stability for KRAS G12D neoantigen detection. Reusability assessment of the NiCo-MS/c-MOF/GCE electrode reveals 94.4% retention of its initial current response after three consecutive cycles (Fig. S9), confirming the stability of the electrode under repeated use. These results confirm that the engineered biosensor demonstrates superior sensitivity, good reproducibility, and long-term stability in detecting KRAS G12D neoantigens.

2.7 Electrochemical detection of HLA-restricted KRAS G12D in cell lysates.

KRAS G12D neoantigen presented by HLA molecules to the cell surface normally exist in the form of HLA-restricted peptide complexes. To validate the analytical efficacy of developed sensor in detecting HLA-restricted KRAS G12D neoantigen complexes, spiking experiments were conducted using COS-7 cell lysates (without endogenous HLA and mutant proteins) with HLA-restricted KRAS G12D complexes at concentrations of 5 nM, 50 nM, and 500 nM. The enrichment of KRAS G12D neoantigen from the complexes in spiked cellular lysate matrices were performed by sequential immunoaffinity-based purification and

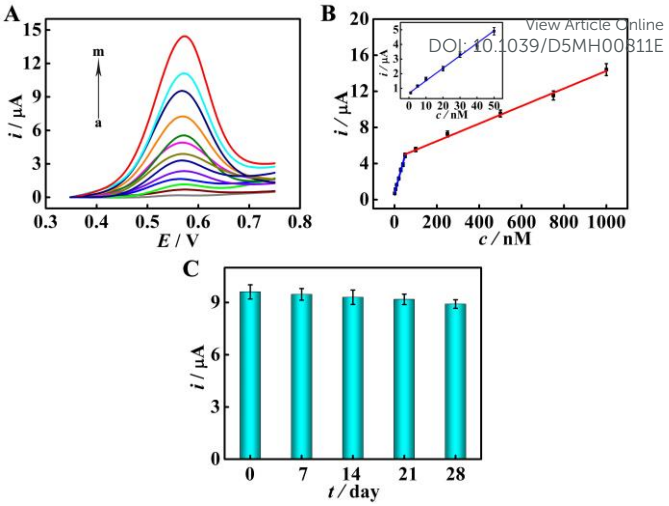

Fig. 5 (A) SWV responses to KRAS G12D neoantigen at incremental concentrations: (a) 0, (b) 1, (c) 5, (d) 10, (e) 20, (f) 30, (g) 40, (h) 50, (i) 100, (j) 250, (k) 500, (l) 750, and (m) 1000 nM; (B) Calibration curve correlating SWV peak currents with neoantigen concentrations (1 nM ~ 1 μM), inset: low-concentration linear curve (1 nM ~ 50 nM); (C) SWV responses for 500 nM KRAS G12D on NiCo-MS/c-MOF/GCE across progressive storage durations. Error bars: SD, n = 3.

membrane filtration processes. As detailed in Fig. 6A, HLA-restricted neoantigen complexes were selectively captured via monoclonal antibodies (W6/32) conjugated to magnetic beads. Following magnetic bead sequestration, the complexes underwent acidic elution (pH 2.8, citric acid buffer), yielding a solution containing HLA-heavy chains (HLA-h), β_2-microglobulin (β_2M), target neoantigens, and detached W6/32 antibodies. Subsequent ultrafiltration (3 kDa MWCO membrane) could selectively enrich KRAS G12D peptides and quantification of neoantigen was performed by the fabricated electrochemical biosensor. As shown in Fig. 6B and 6C, SWV responses of spiked samples exhibit significant enhancement versus blank control, validating the robust anti-interference capability of the methodology for HLA-restricted neoantigen detection in complex matrices. Besides, selectivity experiments for COS-7 cell lysates demonstrate that the HLA-restricted KRAS G12D neoantigen exhibits a markedly stronger current response than the structurally similar non-target peptides (Fig. S11), confirming the high selectivity of the proposed method.

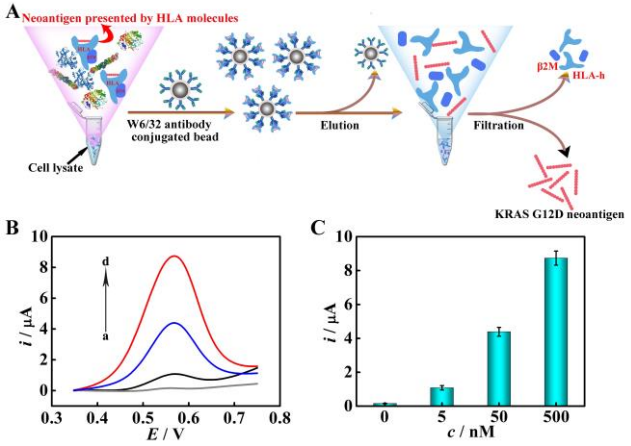

Fig. 6 (A) Workflow schematic of immunoaffinity-based isolation for KRAS G12D neoantigen extraction from HLA-restricted complexes in

spiked lysate matrices; (B) SWV curves and (C) current responses for HLA-restricted complexes quantification: (a) 0, (b) 5 nM, (c) 50 nM, (d) 500 nM. Error bars: SD, n = 3.

3. Conclusions

In summary, this work demonstrates that the NiCo-MS/c-MOF can serve as a superior electrocatalyst to enable ultrasensitive detection of both KRAS G12D neoantigen and HLA-restricted neoantigen complexes within complex biological matrices. The incorporation of metal sulfides via *in situ* vulcanization treatment of c-MOF leads to significant enhancement on its catalytic activity. Upon deriving KRAS G12D neoantigen with OPA/2-ME ligands to generate electrochemically responsive isoindole derivatives, the NiCo-MS/c-MOF nanocomposite exhibits low detection sensitivity. Integrated with immunoaffinity purification and centrifugal ultrafiltration workflows, the developed methodology further allows determination of KRAS G12D neoantigens liberated from HLA-restricted complexes in complex cellular lysate matrices. Our sensor methodology significantly simplifies the analysis procedure compared with cumbersome and labor-intensive mass spectrometry-based means, and provides sufficient sensitivity to quantify HLA-restricted neoantigens. Additionally, the sensor described here can be extended as a universal platform for the determination of other neoantigens, thereby offering promising possibilities for precise and early cancer diagnoses.

Conflicts of interest

There are no conflicts to declare.

Data availability

All relevant data are within the paper and its ESI†.

Acknowledgements

This work was supported by National Natural Science Foundation of China (No. 22174112).

Notes and references

1 H. Khan, M. R. Shah, J. Barek and M. I. Malik, *Trends Anal. Chem.*, 2023, **158**, 116813.
2 R. Liu, X. Ye and T. Cui, *Research*, 2020, **2020**, 7949037.
3 L. Wu and X. Qu, *Chem. Soc. Rev.*, 2015, **44**, 2963–2997.
4 A. W. Purcell, S. H. Ramarathinam and N. Ternette, *Nat. Protoc.*, 2019, **14**, 1687–1707.
5 T. J. Sears, K. H. Lee, M. Pagadala, A. Castro, M. Zanetti and H. Carter, *Cancer Res.*, 2024, **84**, 1204.
6 L. Lybaert, S. Lefever, B. Fant, E. Smits, B. De Geest, K. Breckpot, L. Dirix, S. A. Feldman, W. Van Criekinge, K. Thielemans and S. H. van der Burg, *Cancer Cell*, 2023, **41**, 15–40.
7 L. Lybaert, K. Thielemans, S. A. Feldman, S. H. van der Burg, C. Bogaert and P. A. Ott, *Trends Cancer*, 2023, **9**, 503–519.
8 N. Xie, G. Shen, W. Gao, Z. Huang, C. Huang and L. Fu, *Signal Transduct. Target. Ther.*, 2023, **8**, 9.
9 L. Danilova, V. Anagnostou, J. X. Caushi, J. W. Sidhom, H. Guo and H. Y. Chan, *Cancer Immunol. Res.*, 2018, **6**, 888–899.
10 A. Kacen, A. Javitt, M. P. Kramer, D. Morgenstern, T. Tsaban, M. D. Shmueli, G. C. Teo, F. D. V. Leprevost, E. Barnea, F. Yu and A. Admon, *Nat. Biotechnol.*, 2023, **41**, 239–251.
11 F. Huber, M. Arnaud, B. J. Stevenson, J. Michaux, F. Benedetti, J. Thevenet, S. Bobisse, J. Chiffelle, T. Gehert, M. Müller, H. Pak et al., *Nat. Biotechnol.*, 2024, **1**, 1–13.
12 F. Chen, Z. Zou, J. Du, S. Su, J. Shao, F. Meng, J. Yang, Q. Xu, N. Ding, Y. Yang and Q. Liu, *J. Clin. Invest.*, 2019, **129**, 2056–2070.
13 R. L. Chen, B. C. Hsieh, J. S. Lin and T. J. Cheng, *Biosensors*, 2023, **13**, 485.
14 C. A. Roosa, S. L. Lempke, R. T. Hannan, E. Nicklow, J. M. Sturek, S. E. Ewald and D. R. Griffin, *Adv. Healthc. Mater.*, 2024, **13**, 2400249.
15 P. B. Deroco, D. Wachholz Junior and L. T. Kubota, *Electroanalysis*, 2023, **35**, e202200177.
16 A. Naghashian-Haghighi, B. Hemmateenejad and M. Shamsipur, *Anal. Biochem.*, 2018, **550**, 15–26.
17 C. V. Raju, C. H. Cho, G. M. Rani, V. Manju, R. Umapathi, Y. S. Huh and J. P. Park, *Coord. Chem. Rev.*, 2023, **476**, 214920.
18 K. A. Adegoke and N. W. Maxakato, *Coord. Chem. Rev.*, 2022, **457**, 214389.
19 R. Sheng, Y. Liu, T. Cai, R. Wang, G. Yang, T. Wen and H. Peng, *Chem. Eng. J.*, 2024, **485**, 149913.
20 X. H. Liang, A. X. Yu, X. J. Bo, D. Y. Du and Z. M. Su, *Coord. Chem. Rev.*, 2023, **497**, 215427.
21 H. Louis, M. Patrick, I. O. Amodu, I. Benjamin, I. J. Ikot, G. E. Iniama and A. S. Adeyinka, *Mater. Today Commun.*, 2023, **34**, 105048.
22 N. Kajal, V. Singh, R. Gupta and S. Gautam, *Environ. Res.*, 2022, **204**, 112320.
23 Y. Peng, S. Sanati, A. Morsali and H. García, *Angew. Chem. Int. Ed.*, 2023, **62**, e202214707.
24 K. M. Snook and D. J. Xiao, *Chem*, 2024, **10**, 24–25.
25 X. Shi, Y. Xu, B. Zhao, P. Li, M. Song, J. Jia and G. Lu, *Adv. Mater. Interfaces*, 2021, **8**, 2100586.
26 X. Wang, G. Zhang, W. Yin, S. Zheng, Q. Kong, J. Tian and H. Pang, *Carbon Energy*, 2022, **4**, 246–281.
27 Y. Liu, X. Xu and Z. Shao, *Energy Storage Mater.*, 2020, **26**, 1–22.
28 J. Du, F. Li and L. Sun, *Chem. Soc. Rev.*, 2021, **50**, 2663–2695.
29 K. Srinivas, Y. Chen, X. Wang, M. Karpuraranjith, W. Wang, Z. Su, W. Zhang and D. Yang, *ACS Sustain. Chem. Eng.*, 2021, **9**, 1920–1931.
30 M. Chen, T. Zeng, L. Luo, L. Wu, S. Fu, J. Shen and B. Xi, *J. Alloys Compd.*, 2024, **984**, 173969.
31 E. Tran, P. F. Robbins, Y. C. Lu, T. D. Prickett, J. J. Gartner, L. Jia, A. Pasetto, Z. Zheng, S. Ray, E. M. Groh and I. R. Kriley, *N. Engl. J. Med.*, 2016, **375**, 2255–2262.
32 A. Althaiban, A. Thyagarajan and R. Prakash Sahu, *Mini Rev. Med. Chem.*, 2023, **23**, 953–961.
33 H. Yoon, S. Lee, S. Oh, H. Park, S. Choi and M. Oh, *Small*, 2019, **15**, 1805232.
34 Y. Jiang, G. Zhang, H. Zhang, J. He, J. Jia, Y. Zhang, L. Zhu, M. Shi, Y. Du, J. Zhao and J. Cao, *J. Alloys Compd.*, 2024, **1005**, 176101.
35 J. Ding, X. Q. Liu, L. Wang and Y. B. Zhu, *New J. Chem.*, 2024, **48**, 4184–4190.
36 X. Shi, R. Hua, Y. Xu, T. Liu and G. Lu, *Sustain. Energy Fuels*, 2020, **4**, 4589–4597.
37 Y. X. Shi, Y. Wu, S. Q. Wang, Y. Y. Zhao, T. Li, X. Q. Yang and T. Zhang, *J. Am. Chem. Soc.*, 2021, **143**, 4017–4023.

View Article Online
DOI: 10.1039/D5MH00811E

38 J. Sun, L. Guo, X. Sun, J. Zhang, Y. Liu, L. Hou and C. Yuan, *J. Mater. Chem. A*, 2019, **7**, 24788–24791.
39 Y. Wang, Y. Y. Xue, L. T. Yan, H. P. Li, Y. P. Li, E. H. Yuan, M. Li, S. N. Li and Q. G. Zhai, *ACS Appl. Mater. Interfaces*, 2020, **12**, 24786–24795.
40 Q. Qian, Y. Li, Y. Liu, L. Yu and G. Zhang, *Adv. Mater.*, 2019, **31**, 1901139.
41 B. Niu, M. Liu, X. Li, H. Guo and Z. Chen, *ACS Appl. Mater. Interfaces*, 2023, **15**, 13319–13331.
42 M. Ko, L. Mendecki, A. M. Eagleton, C. G. Durbin, R. M. Stolz, Z. Meng and K. A. Mirica, *J. Am. Chem. Soc.*, 2020, **142**, 11717–11733.
43 Y. L. Li, J. J. Zhou, M. K. Wu, C. Chen, K. Tao, F. Y. Yi and L. Han, *Inorg. Chem.*, 2018, **57**, 6202–6205.
44 P. He, Y. Xie, Y. Dou, J. Zhou, A. Zhou, X. Wei and J. R. Li, *ACS Appl. Mater. Interfaces*, 2019, **11**, 41595-41601.
45 J. Lin, H. Zhou, R.S. Amin, A.E. Fetohi, K.M. El-Khatib, C. Wang, L. Guo and Y. Wang, *Inorg. Chem. Front.*, 2023, **10**, 1294-1304.
46 W. A. El-Said, R. M. Qaisi, V. Placide and J. W. Choi, *Spectrochim. Acta A: Mol. Biomol. Spectrosc.*, 2022, **267**, 120517.
47 A. Kousar and T. Laurila, *J. Electroanal. Chem.*, 2024, **965**, 118374.
48 A. Chapin, J. Han and R. Ghodssi, *Methods Protoc.,* 2023, **6**, 6.